Asymmetric thermocapillarity-based pump: Concept and exactly solved model

Darren Crowdy,[1,*] Michael Mayer,[1] and Marc Hodes[2]
[1]*Department of Mathematics, Imperial College London, 180 Queen's Gate, London SW7 2AZ, United Kingdom*
[2]*Department of Mechanical Engineering, Tufts University, 200 College Avenue, Medford, Massachusetts 02155, USA*

(Received 14 February 2023; accepted 22 August 2023; published 28 September 2023)

A mechanism for a microfluidic pump that leverages alternating adverse and favorable thermocapillary stresses along menisci in a (periodically) fully developed transverse flow in a microchannel is exemplified. The transverse ridges are the interdigitated teeth of cold and hot (isothermal) "combs" and free surface menisci span the interstitial regions between them. The teeth are asymmetrically positioned so that the widths of adjacent menisci differ. This architecture is essentially that of the theoretical pump proposed by Adjari [Phys. Rev. E **61**, R45(R) (2000)] but exploits thermocapillarity rather than electro-osmotic slip to drive unidirectional pumping. A theoretical model of the multiphysics pumping mechanism is given that is solved in closed form. Two explicit formulas for the pumping speed are provided. One is derived from the exact solution to the full problem; the other follows from the reciprocal theorem for Stokes flow combined with an exact solution to a distinct problem resolving apparent slip over superhydrophobic surfaces [D. G. Crowdy, Phys. Fluids **23**, 072001 (2011)]. A conceptual design of the pump is also outlined; this involves no moving parts, requires no external driving pressure, and pumps a continuous stream of liquid through a microchannel, as opposed to a series of discrete droplets. Since there is only a periodic component of the pressure field the microchannel could be made arbitrarily long and the menisci, which would be essentially flat, are more robust than for conventional pressure-driven flow.

DOI: 10.1103/PhysRevFluids.8.094201

I. INTRODUCTION

In the design of microfluidic devices that serve as, for example, a laboratory on a chip, there is a need for precise control of small volumes of liquid [1,2]. Pumping liquid along such a device, typically at very low Reynolds number, is a basic requirement and microfluidic pumps of various kinds have been devised mostly based on the use of pressure differences or electric fields, the latter manifesting themselves as electro-osmosis, electrowetting, and electrohydrodynamics [1,2].

An interesting theoretical pumping mechanism was advanced by Adjari [3] who proposed an electro-osmotic pump driven by ac fields where broken symmetries of the electrode geometry produce nonzero time-averaged electro-osmotic slip velocities at the electrodes, causing

*Corresponding author: d.crowdy@imperial.ac.uk

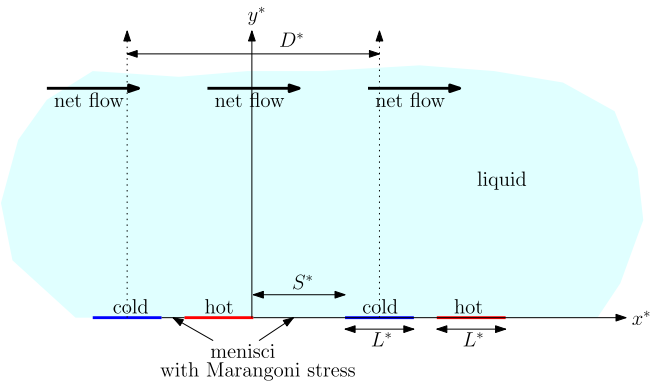

FIG. 1. Dimensional geometry of the multiphysics problem studied here. Two periods are shown of a periodic array of isothermal hot and cold plates of lengths L^* alternating with a period of D^* in the x^* direction. At zero Reynolds number and zero thermal Péclet number, it is shown that a net pumping of the overlying liquid in the direction indicated can be expected. The pumping speed depends on the meniscus length S^* shown here.

unidirectional pumping of the liquid. The mechanism for this theoretical pump has now been tested experimentally [4–6] and numerical simulations of the underlying mechanism have also been performed [7]. Squires and Bazant [8] have since explored the use of broken symmetries in induced charge electro-osmosis and electrophoresis in more general geometrical settings. Adjari [3] ends his paper by emphasizing that it is the intrinsic asymmetry of the device architecture that gives rise to the pumping and suggests that other physical effects, beyond the electro-osmotic mechanism he specifically advanced, are viable.

In the present paper, a different type of pump is advanced, exploiting the same asymmetry in the same device architecture envisaged by Adjari [3] but relying on Marangoni stresses induced by thermocapillarity as its essential physical mechanism. A key objective is to demonstrate the viability of the mechanism by constructing a theoretical model of the proposed pump, one that turns out to be exactly solvable in mathematical form. This model multiphysics problem is shown in Fig. 1. A periodic array of isothermal hot and cold plates, all of length L^*, alternate with period D^* in the x^* direction. Figure 1 shows two periods of this periodic array and a significant feature is that there is both a hot and cold plate in each period window. Importantly, there are also two free-surface menisci in each period window which, as indicated in Fig. 1, are generally of different length; this is quantified by the meniscus length S^* shown in Fig. 1 (the length of the other meniscus is then $D^* - 2L^* - S^*$). The surface tension on these menisci varies along them with a linear dependence on the local temperature. This causes Marangoni stresses that incite a nontrivial flow in the overlying liquid and, as will be shown here by solving the multiphysics problem analytically, a net pumping of the liquid far away from the plates assuming zero Reynolds number and zero thermal Péclet number. Section IX gives a summary of the analytical results: formula (71) provides an explicit, closed-form representation of both the temperature field and velocity field in this cross section; this section also summarizes two equivalent closed-form expressions (72) and (73), for the pumping speed.

It is both remarkable and valuable that the solution of a multiphysics problem of this kind taking place in a nontrivial geometry admits such a concise analytical representation. This solution is valuable not only in exemplifying a basic transport mechanism, but also because it relies on certain technical ingredients that are intrinsic to the device architecture and not specific to the physical driving mechanism. This includes a conformal mapping function to the domain cross section stated in (71) from a convenient annular preimage domain, as well as a reciprocal theorem result, embodied in (58), that applies in principle to many other physical settings taking place in the same geometry. The motivation for studying this two-dimensional multiphysics problem is given in Sec. II, where it

is shown how the problem arises from consideration of two "combs," one hot and another cold, having interdigitated teeth. In cross section, these teeth form the hot and cold plates shown in Fig. 1. Indeed, in Sec. II a conceptual design of a pumping device based on the essential mechanism quantified in this paper is set out (such a pump has not yet been built, however).

This is not the first time thermal effects have been proposed as a microfluidic pumping mechanism and thermocapillarity can play an important role in small-scale fluid manipulation of discrete droplets [9]. Kataoka and Troain [10] utilized thermocapillarity along a silicone-oil film on a surface patterned with alternating hydrophilic and hydrophobic stripes to direct liquid motion. Würger [11] theoretically studied the autopropulsion of a "spherical floater." Specifically, a sphere containing an active and off-center heat source generates a temperature field that is symmetric about the heat source but asymmetric about the sphere itself to drive propulsion. A review article by Karbalaei *et al.* [12] surveys a range of other applications of thermocapillarity in microfluidics.

As to exploiting thermocapillarity to drive a net flow, Frumkin *et al.* [13] exploited it to pump (tap) water through a 0.5 mm$\times$1 mm cross-section, 26-mm-long channel in a closed loop at a maximum velocity of 15 μm/s when a 3 °C temperature difference drove the flow. The pump cell consisted of two plates. The bottom one was a flat, no-slip surface and the top one was the same footprint but it contained a circular opening to expose a free surface. A temperature gradient across the free surface generated a pressure difference across the microchannel to drive the flow. Additionally, Frumkin *et al.* [13] used a similar concept to propel a surface swimmer in the form of a thin annulus floating on a film of water with a free surface corresponding to the hole in its middle. A heat-absorbing annular stripe on one side of the annulus, irradiated by a halogen lamp, imposed a temperature gradient and thus thermocapillary stress along the free surface to drive propulsion. Also, in an experiment on Maragoni-Bérnard convection, Strook *et al.* [14] drove a net flow of a film of oil along a heated surface with an asymmetric, ratchetlike topography.

Thermocapillarity in superhydrophobic microchannels has also been considered. In a theoretical study, Baier *et al.* [15] imposed a unidirectional temperature gradient along (parallel or transverse) ridge-type superhydrophobic microchannels to drive a flow of water through them at several mm/s for a 10 °C/m temperature gradient. This flow configuration limits the streamwise length of the pump to the distance required for the liquid to freeze as results from the requisite decreasing (increasing) temperature (surface tension) in the streamwise direction, a constraint not imposed by the pumping mechanism considered here. Experiments by Amador *et al.* [16] demonstrated the concept advanced by Baier *et al.* [15]. More recently, in a thin (circular footprint) film of water bounded by a superhydrophobic (smooth) surface on its top (bottom), Gao *et al.* [17] exploited thermocapillarity to generate flow via an "optothermal" effect, i.e., using light absorption to heat the superhydrophobic surface. Their accompanying numerical model utilized an apparent-slip boundary condition for along the superhydrophobic surface and captured buoyancy effects.

The degradation in lubrication due to the effects of adverse thermocapillary stresses on pressure-driven flow through heated, superhydrophobic microchannels has also been quantified [18,19]. Yariv and co-workers published a series of papers [20–23] on the effects of thermocapillarity on flows through heated, superhydrophobic microchannels. First, Yariv [20] resolved the cross flow driven by a constant temperature gradient imposed along parallel ridges. Second, Yariv and Crowdy [21] resolved two asymptotic limits relevant to the transverse-ridge problem considered by Baier *et al.*, namely, when the ratio of the ridge period to channel height is $\gg 1$ or $\ll 1$. Third, Yariv and Crowdy [22] captured the effect of menisci protruding by 90° into the channel in the small solid fraction limit for the longitudinal-ridge problem considered by Baier *et al.* [15]; Yariv and Kirk [23] did the same in the small gas fraction limit. Finally, Tomlinson *et al.* [24] captured the effects of thermocapillarity on Nusselt number in diabatic, superhydrophobic microchannels.

In the design of heat pipes the use of electrowetting mechanisms acting on discrete droplets has also been proposed [25,26] as a means to pump condensate to the evaporator. Such proposals aim to overcome transport limits associated with use of capillary pressure in more traditional wicks, i.e., enable a heat pipe to be arbitrarily long rather than constrained by a performance limit such as the capillary limit. Another advantage of the pump put forward here is that it pumps a continuous

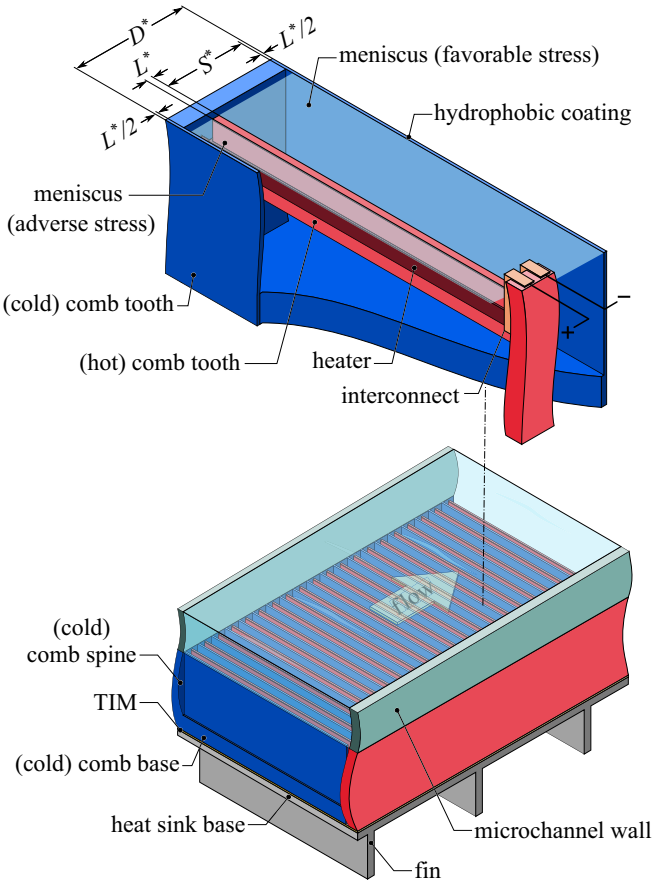

FIG. 2. A conceptual design proposition for the thermocapillary pump in a microchannel flow configuration.

stream of liquid without the need for the discretization into droplets necessary to facilitate contact angle differentials fore and aft on which such electrowetting devices rely.

II. PHYSICAL DESCRIPTION OF THE PUMP

The motivation for studying the multiphysics problem shown in Fig. 1 derives from Fig. 2 which summarizes a conceptual design of a pumping device and shows only the lower half of the up-down symmetrical structure of the proposed pump. It should be emphasized that this is a design proposition; the authors have not built such a device. Its key components are two (asymmetrically) interdigitated "combs," a cold (blue) one having a base, spine, and teeth (ridges, or what will be called plates in the theoretical modeling) and a hot (red) one without a base. Both might be microfabricated in a high-thermal-conductivity material (say, silicon) such that they are essentially isothermal, and have a hydrophobic coating on their tips. The base of the cold comb might be attached to a heat sink via a layer of thermal interface material (TIM) in order to maintain it near ambient temperature. (Alternatively, a subambient temperature may be obtained by inserting a thermoelectric module between the TIM and heat sink.) A current driven through thin-film heaters deposited on the teeth of the hot comb (say, by sputtering TiW) could maintain the requisite temperature excursion relative to the cold comb. The teeth of the hot comb are deliberately shorter than those of cold one to minimize the leakage of heat to the cold one, i.e., to force virtually all of the heat transferred from the hot ridge to the cold one to be through the liquid.

The objective is to achieve liquid pumping in the direction parallel to the spine of each comb using thermocapillary-induced Marangoni stresses. It is assumed that, along the menisci between the interdigitated teeth of each comb, surface tension $\sigma^\star$ depends on temperature $T^\star$ according to a linear relation

$$\sigma^\star = \sigma_c^\star - \beta^\star(T^\star - T_c^\star), \tag{1}$$

where $\sigma_c^\star$ is the surface tension of the liquid at reference temperature $T_c^\star$ and the coefficient $\beta^\star$ is associated with the chosen liquid. Since Marangoni stresses are dependent only on gradients of surface tension the values of $\sigma_c^\star$ and $T_c^\star$ do not appear in our subsequent analysis. In the modeling to follow, gravity is neglected and the (thermal) Péclet number is taken to be zero so that all of the heat emerging from the hot ridge conducts into and through the liquid to the cold one but there is no advection (however, in Sec. X, the effect of a nonzero thermal Péclet number is examined numerically). A (one-way) coupling of the temperature field with the liquid motion is nevertheless caused by the nonuniform temperature varying the surface tension on the menisci between the interdigitated teeth of the combs according to (1). This induces Marangoni stresses on the viscous liquid.

A crucial feature is the asymmetry in the spacing between the ridges. As shown in the upper schematic in Fig. 2, and whose cross section is shown in Fig. 1, the meniscus subjected to adverse thermocapillary stress [that is, where the temperature (surface tension) increases (decreases) in the flow direction] is shorter than the one subjected to a favorable stress. This leads to a net pumping of the fluid in the direction shown, as will be demonstrated analytically in this paper by solving the theoretical model advanced in the next section. Since the flow is hydrodynamically and thermally fully developed periodically there is solely a periodic component of the pressure and temperature fields and the rate of heat transfer into the liquid along the tip of a hot tooth equals that transferred out of it along the tip of a cold one.

III. DESCRIPTION OF THE THEORETICAL MODEL

The Stokes equations governing the two-dimensional liquid motion can be represented in stream-function form as

$$\nabla^4 \psi^\star = 0, \tag{2}$$

where $u^\star$ and $v^\star$, the velocities in the $x^\star$ and $y^\star$ directions, are related to the stream function $\psi^\star$ by

$$u^\star = \frac{\partial \psi^\star}{\partial y^\star}, \quad v^\star = -\frac{\partial \psi^\star}{\partial x^\star}. \tag{3}$$

The assumption that the thermal Péclet number vanishes means that the temperature field is governed by Laplace's equation,

$$\nabla^2 T^\star = 0. \tag{4}$$

The two plates are taken to be no-slip surfaces with the plate occupying $y^\star = 0$, $-L^\star < x^\star < 0$ held at temperature $T^\star = \Delta T^\star$. The other plate is held at $T^\star = 0$. On the two menisci, a thermal Marangoni condition couples the temperature field and velocity field via

$$\mu^\star \frac{\partial u^\star}{\partial y^\star} = -\frac{\partial \sigma^\star}{\partial x^\star} = \beta^\star \frac{\partial T^\star}{\partial x^\star}. \tag{5}$$

The velocity is assumed to reach some constant value, $U_\infty^\star$, far from the composite boundary. The problem can be cast into dimensionless form using

$$z = \frac{z^\star}{D^\star}, \quad L = \frac{L^\star}{D^\star}, \quad S = \frac{S^\star}{D^\star}, \quad (u, v) = \frac{\mu^\star}{\beta^\star \Delta T^\star}(u^\star, v^\star),$$
$$\psi = \frac{\psi^\star D^\star \mu^\star}{\beta^\star \Delta T^\star}, \quad p = \frac{p^\star D^\star}{\beta^\star \Delta T^\star}, \quad T = \frac{T^\star}{\Delta T^\star}, \tag{6}$$

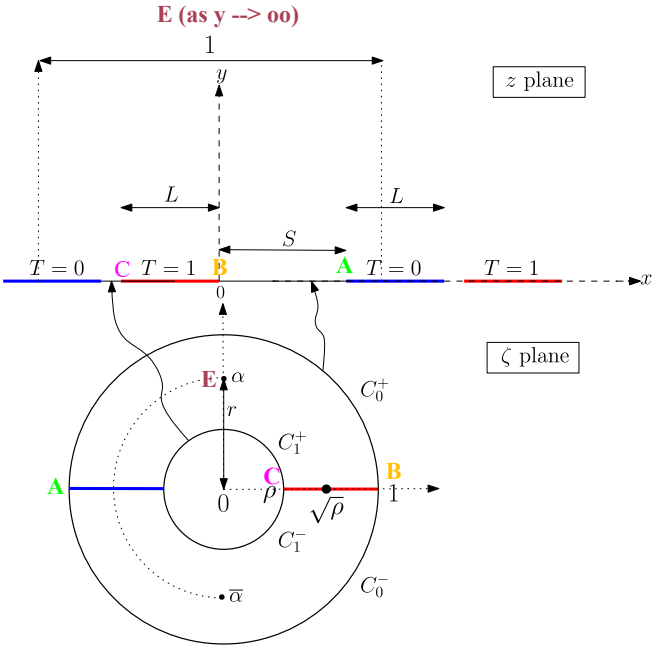

FIG. 3. A periodic array of hot and cold plates alternating with unit period in the x direction. Points in the upper-half annulus, $\rho < |\zeta| < 1$, $\mathrm{Im}[\zeta] > 0$, are in one-to-one correspondence with points in a principal period window, $-1/2 < x < 1/2$, $y > 0$. The point $\alpha = ir$ in the upper half of the annulus $\rho < |\zeta| < 1$ maps to $y \to \infty$. The plates have equal length L and a cold plate is located at separation S to the right of a hot plate; the two menisci therefore have different lengths except when $S = (1 - 2L)/2$. The values of ρ and r in the ζ plane control L and S in the physical z plane with $r = \sqrt{\rho}$ corresponding to the left-right symmetric case where $S = (1 - 2L)/2$.

where $p^\star$ is the liquid pressure. All the equations stated earlier remain largely unchanged, the only adjustments being to the constant temperature condition on the hot plate, where now $T = 1$, and the Marangoni condition, where now

$$\frac{\partial u}{\partial y} = -\frac{\partial T}{\partial x}. \tag{7}$$

The dimensionless problem additionally comes with two dimensionless parameters, i.e., $\mathrm{Re} = \rho^\star U^\star D^\star/\mu^\star$ and $\mathrm{Pe} = U^\star D^\star/\alpha^\star$, the Reynolds number and thermal Péclet number, respectively; here $\rho^\star$ is the liquid's density and $\alpha^\star$ its thermal diffusivity. These two dimensionless parameters are assumed to be zero as stated earlier, but their definition is included for discussion later.

Figure 3 shows a schematic of the flow domain after the aforementioned nondimensionalization. It shows how the nondimensional plate separation parameter S is defined as the length of the meniscus to the right of a typical hot plate; the meniscus length to its left will then be $1 - 2L - S$. It is important to note that while we have taken both plates to have the same length L, the lengths of these two menisci are generally different. When the two menisci have the same length, so that $S = 1 - 2L - S$, or $S = (1 - 2L)/2$, no liquid pumping is expected due to the left-right symmetry of the configuration in that case (Marangoni effects will only introduce mixing). But when the two menisci have different lengths it will be shown, by solving analytically for the temperature field and, subsequently, the induced Stokes flow of the viscous liquid, that a net pumping of the liquid is achieved.

The problem just described differs from the transverse-ridge problem studied by Baier *et al.* [15] in several significant ways and it is worth emphasizing these. First, each period window here

necessarily contains two menisci, not just one: this is critical for pumping. Second, Baier *et al.* [15] impose isothermal ridges, as we do, but their temperature decreases monotonically in the streamwise direction unlike the problem studied here. Third, the analysis to follow includes a full resolution of the temperature gradients along menisci while Baier *et al.* [15] impose one. Finally, in a numerical part of their study, Baier *et al.* [15] resolve the effects of inertia and advection; in the present study, the zero Péclet number assumption needed to find fully analytical solutions is relaxed in the numerical computations in Sec. IX, but inertia is still ignored.

IV. CONFORMAL MAPPING

By the unit periodicity of the arrangement, it is enough to consider the flow in a principal period window $-1/2 < x < 1/2$, $y > 0$. The analysis to follow will make use of a conformal mapping already used in a study [27] of superhydrophobic surfaces (characterized by shear-free menisci existing between no-slip plates) but will be deployed here in a different context. The advantage of introducing a parametric conformal mapping variable ζ is that both the temperature problem and the flow problem can be solved explicitly in terms of it.

The relevant mapping, from a parametric annulus $\rho < |\zeta| < 1$, is [27,28]

$$z = Z(\zeta) = -\frac{\mathrm{i}}{2\pi}\log\left[R\,\frac{P(\zeta/\alpha,\rho)P(\zeta\alpha,\rho)}{P(\zeta/\overline{\alpha},\rho)P(\zeta\overline{\alpha},\rho)}\right], \tag{8}$$

where $\alpha = \mathrm{i}r$ for $\rho < r < 1$, and

$$P(\zeta,\rho) \equiv (1-\zeta)\prod_{n=1}^{\infty}(1-\rho^{2n}\zeta)(1-\rho^{2n}/\zeta). \tag{9}$$

This important function (9) can be identified with the *prime function* [27,28] associated with the concentric annulus $\rho < |\zeta| < 1$. The constant R is chosen to be

$$R = \frac{P(1/\overline{\alpha},\rho)P(\overline{\alpha},\rho)}{P(1/\alpha,\rho)P(\alpha,\rho)}, \tag{10}$$

which ensures that $Z(1) = 0$. Under the mapping (8), the upper-half annulus, $\rho < |\zeta| < 1$, $\mathrm{Im}[\zeta] > 0$, is in one-to-one correspondence with the liquid in a principal period window as shown in Fig. 3. The upper unit semicircle, denoted by C_0^+, maps to one of the menisci (with the lower half of the unit circle, denoted by C_0^-, also mapping to the same meniscus); the upper semicircle of radius ρ, denoted by C_1^+, maps to the other meniscus (with the lower half of the radius ρ circle, denoted by C_1^-, also mapping to the same meniscus). The segment $[\rho, 1]$ on the positive real axis is transplanted to the hot plate in the period window held at temperature ΔT, and the portion $[-1, -\rho]$ on the negative real axis maps to the cold plate held at zero temperature.

The mapping (8) depends on the two real positive parameters ρ and r satisfying $0 \leqslant \rho < 1$, $\rho < r < 1$. These two mathematical parameters are related to the two geometrical parameters L and S also shown in Fig. 3. Indeed, as indicated in Fig. 3, the mapping is such that

$$Z(-1) = S, \quad Z(-\rho) = S + L, \tag{11}$$

and these two equations provide nonlinear algebraic relations between the parametric pair $\{\rho, r\}$ and the geometrical pair $\{L, S\}$. It will then follow, from the functional form of the mapping, that

$$Z(\rho) = -L. \tag{12}$$

One can pick $\{\rho, r\}$ and find $\{L, S\}$ using the explicit relations (11). Alternatively, if the pair $\{L, S\}$ is specified, then (11) must be solved (e.g., using a simple Newton method) for the corresponding $\{\rho, r\}$.

It is worth remarking that the requirement that the plates be of equal length is not necessary and can easily be relaxed. Mathematically, this is done simply by allowing the parameter α in (8) to

move off the imaginary axis so that it is a more general point in the upper-half annulus $\rho < |\zeta| < 1$, $\mathrm{Im}[\zeta] > 0$.

V. SOLUTION FOR THE TEMPERATURE FIELD

The nondimensional version of (4) governing the temperature T is

$$\nabla^2 T = 0, \quad -\frac{1}{2} < x < \frac{1}{2}, \quad y > 0. \tag{13}$$

The two menisci are taken to be adiabatic so that

$$\frac{\partial T}{\partial y} = 0 \text{ on the menisci.} \tag{14}$$

The hot and cold plate are such that

$$T = \begin{cases} 1 & \text{on the hot plate} \\ 0 & \text{on the cold plate.} \end{cases} \tag{15}$$

It is assumed that no heat enters the system from the far field so that heat entering each period window through the heated plate is conducted away through the cooler plate.

The temperature field $T(x, y)$ will be found by determining the analytic function

$$w(z) = \chi + \mathrm{i}T, \quad z = x + \mathrm{i}y, \tag{16}$$

where χ is the harmonic conjugate to T in the liquid region and the usual complex variable $z = x + \mathrm{i}y$ has been introduced. On use of one of the Cauchy-Riemann equations, namely,

$$\frac{\partial \chi}{\partial x} = \frac{\partial T}{\partial y}, \tag{17}$$

then (14) says that

$$\chi = \text{const on the menisci.} \tag{18}$$

Actually, $w(z)$ will be found parametrically as a function of ζ. The solution for the composed function $W(\zeta) \equiv w(Z(\zeta))$ is easily confirmed to be the analytic function

$$W(\zeta) = \mathrm{i} - \frac{1}{\pi} \log \zeta. \tag{19}$$

It is clear that $\mathrm{Re}[W(\zeta)] = \chi = -(\Delta T/\pi) \log |\zeta|$ is constant on $|\zeta| = 1, \rho$, which means that (18) is satisfied. It can also be checked that

$$\mathrm{Im}[W(\zeta)] = T = 1 - \frac{\arg[\zeta]}{\pi} = \begin{cases} 1, & \arg[\zeta] = 0 \\ 0, & \arg[\zeta] = \pi, \end{cases} \tag{20}$$

which means that (15) is satisfied because the positive and negative portions of the real ζ axis inside the annulus $\rho < |\zeta| < 1$ correspond to the hot and cold plates, respectively.

VI. SOLUTION FOR THE FLOW

Solving for the incompressible Stokes flow generated in the upper half plane is more challenging but, again, a parametric solution using the ζ variable is possible. The flow has an associated biharmonic stream function that can be represented as

$$\psi(x, y) = \mathrm{Im}[\bar{z} f(z) + g(z)], \quad z = x + \mathrm{i}y, \tag{21}$$

where the two analytic functions $f(z)$ and $g(z)$ are known as Goursat functions. The following relations between the Goursat functions and the physical variables can be derived [29]:

$$4f'(z) = p - \mathrm{i}\omega, \quad u - \mathrm{i}v = -\overline{f(z)} + \bar{z}f'(z) + g'(z),$$
$$e_{11} + \mathrm{i}e_{12} = z\overline{f''(z)} + \overline{g''(z)}, \tag{22}$$

where ω is the vorticity, e_{ij} is the rate-of-strain tensor, and primes denote differentiation with respect to z. Since liquid penetrates neither the plates nor the menisci the x axis must be a streamline and the choice

$$g(z) = -zf(z) \tag{23}$$

ensures this. It follows from use of (23) in (22) that

$$U(x) = -f(z) - \overline{f(z)}, \quad H \equiv f(z) + z\overline{f'(z)} + \overline{g'(z)} = f(z) - \overline{f(z)}, \tag{24}$$

where $U(x)$ denotes the slip velocity in the x direction on $y = 0$. The quantity H is useful because the Marangoni condition on the interface can be written in terms of it [29,30]:

$$-2\mathrm{i}\frac{dH}{dx} = -\frac{\partial\sigma}{\partial x} = \frac{\partial T}{\partial x}, \tag{25}$$

where we have used (1). It follows on integration of (25) with respect to x that

$$-2\mathrm{i}H = T, \tag{26}$$

where an additive degree of freedom in the specification of $f(z)$ has allowed us to set a constant of integration to zero without loss of generality. But on use of (24) this implies that, on the menisci,

$$4\mathrm{Im}[f(z)] = T, \quad -2\mathrm{Re}[f(z)] = U \quad \text{or} \quad f(z) = -\frac{U}{2} + \frac{\mathrm{i}T}{4}. \tag{27}$$

Since the solution to the temperature problem has already been found, the temperature and, hence, the imaginary part of $f(z)$ on the menisci are known quantities. On defining a modified analytic function $h(z)$ via

$$f(z) = \frac{\mathrm{i}}{4}h(z) \tag{28}$$

and introducing $\mathcal{H}(\zeta) \equiv h(Z(\zeta))$, we can write

$$\mathrm{Re}[\mathcal{H}(\zeta)] = \begin{cases} \mathrm{Re}[W(\zeta)] = 1 - \theta/\pi, & \zeta = e^{\mathrm{i}\theta},\ 0 \leqslant \theta \leqslant \pi \\ \mathrm{Re}[W(\zeta)] = 1 - \theta/\pi, & \zeta = \rho e^{\mathrm{i}\theta},\ 0 \leqslant \theta \leqslant \pi. \end{cases} \tag{29}$$

Thus the real part of $\mathcal{H}(\zeta)$ is known on the two semicircular boundaries of the annulus in the upper half plane. On the plates, which are solid surfaces, we must impose a no-slip condition; this means that $U = 0$ there and

$$\mathrm{Im}[\mathcal{H}(\zeta)] = 0, \quad \text{for } \overline{\zeta} = \zeta. \tag{30}$$

The latter condition implies

$$\overline{\mathcal{H}}(\zeta) = \mathcal{H}(\zeta), \tag{31}$$

where we have introduced the Schwarz conjugate function to $\mathcal{H}(\zeta)$ defined by $\overline{\mathcal{H}}(\zeta) \equiv \overline{\mathcal{H}(\overline{\zeta})}$. Relation (31) can be used to infer the boundary data on the real part of $\mathcal{H}(\zeta)$ on the lower-half semicircles C_0^-, C_1^-. Suppose $\zeta \in C_0^-$, or $\zeta = e^{\mathrm{i}\theta}$ for $-\pi \leqslant \theta \leqslant 0$, then $\overline{\zeta} \in C_0^+$; similarly, if $\zeta \in C_1^-$, or $\zeta = \rho e^{\mathrm{i}\theta}$, then $\overline{\zeta} \in C_1^+$. It can therefore be inferred that

$$\mathrm{Re}[\mathcal{H}(\zeta)] = \mathrm{Re}[\overline{\mathcal{H}(\zeta)}] = \mathrm{Re}[\mathcal{H}(\overline{\zeta})]$$
$$= \begin{cases} 1 + \theta/\pi, & \zeta = e^{\mathrm{i}\theta},\ -\pi \leqslant \theta \leqslant 0 \\ 1 + \theta/\pi, & \zeta = \rho e^{\mathrm{i}\theta},\ -\pi \leqslant \theta \leqslant 0. \end{cases} \tag{32}$$

The first equation follows from the fact that the real parts of complex conjugate quantities are equal, in the second equality (31) has been used, while the third equality follows on use of (29). By these considerations the problem has been reduced to a so-called modified Schwarz problem on the concentric annulus [28,31]: this is the problem of finding a (single-valued) analytic function in the annulus given its real part on the boundaries. In this case, (29) furnishes the real part of $\mathcal{H}(\zeta)$ on the upper half circles C_0^+, C_1^+ and (32) on the lower half circles C_0^-, C_1^-. There is a solvability condition on these specified data for such a single-valued function $\mathcal{H}(\zeta)$ to exist [28,31]—it will appear later in (41); however, it is easily checked that the data in (29) and (32) satisfy this condition.

One way to solve this modified Schwarz problem is to use the so-called Villat integral formula [28,31]. However, another approach is more convenient. Since $\mathcal{H}(\zeta)$ is known to be analytic and single valued in the annulus $\rho < |\zeta| < 1$ it can be written as the convergent Laurent series

$$\mathcal{H}(\zeta) = \sum_{n=0}^{\infty} a_n \zeta^n + \sum_{n=1}^{\infty} \frac{a_{-n}\rho^n}{\zeta^n}. \tag{33}$$

The coefficients $\{a_n\}$ must be real because of condition (31). It is also known that $H(\zeta)$ satisfies boundary conditions of the form

$$\mathrm{Re}[\mathcal{H}(\zeta)] = \begin{cases} d(\zeta) & \text{on } |\zeta| = 1 \\ e(\zeta) & \text{on } |\zeta| = \rho, \end{cases} \tag{34}$$

where it is assumed that the data on each circle have Fourier series representations of the form

$$d(\zeta) = \sum_{n=-\infty}^{\infty} d_n e^{\mathrm{i}n\theta}, \quad e(\zeta) = \sum_{n=-\infty}^{\infty} e_n e^{\mathrm{i}n\theta}, \tag{35}$$

where $d_{-n} = \overline{d_n}$ and $e_{-n} = \overline{e_n}$. Then on substitution of (33) into the first boundary condition on $|\zeta| = 1$ and on equating positive powers of ζ it follows that

$$a_n + \overline{a_{-n}}\rho^n = 2d_n, \quad n \geqslant 1. \tag{36}$$

The coefficients of the negative powers give no new information. On setting $\zeta \mapsto \rho\zeta$ and substituting into the second boundary condition on $|\zeta| = \rho$ then, after equating positive powers of ζ, it is found that

$$a_n\rho^n + \overline{a_{-n}} = 2e_n, \quad n \geqslant 1. \tag{37}$$

Solving (36) and (37) then gives

$$a_n = \frac{2(d_n - \rho^n e_n)}{1 - \rho^{2n}}, \quad n \geqslant 1, \tag{38}$$

and

$$a_{-n} = \frac{2\overline{e_n} - 2\rho^n \overline{d_n}}{1 - \rho^{2n}}, \quad n \geqslant 1. \tag{39}$$

It must also be true that

$$\mathrm{Re}[a_0] = d_0 \tag{40}$$

and, for consistency, the data must satisfy

$$e_0 = d_0 \tag{41}$$

which is precisely the solvability condition mentioned earlier.

The next piece of information needed is the following Fourier cosine series:

$$\frac{1}{2} + \sum_{n\geqslant 1} \frac{2((-1)^n - 1)}{(\pi n)^2} \cos n\theta = \begin{cases} \theta/\pi, & 0 \leqslant \theta \leqslant \pi \\ -\theta/\pi, & -\pi \leqslant \theta \leqslant 0, \end{cases} \tag{42}$$

which follows from a straightforward calculus exercise. This means that, for the problem considered here,

$$d(\zeta) = e(\zeta) = \frac{1}{2} - \sum_{n\geqslant 1} \frac{((-1)^n - 1)}{(\pi n)^2}(e^{\mathrm{i}n\theta} + e^{-\mathrm{i}n\theta}), \tag{43}$$

from which the required coefficients are read off as

$$d_0 = e_0 = \frac{1}{2}, \quad d_n = e_n = \frac{1-(-1)^n}{(\pi n)^2}. \tag{44}$$

Therefore, use of these in (38)–(40) yields

$$\begin{aligned} a_0 &= \frac{1}{2}, \\ a_n = a_{-n} &= \frac{2d_n(1-\rho^n)}{1-\rho^{2n}} = \frac{2d_n}{1+\rho^n} = \frac{2}{1+\rho^n}\left(\frac{1-(-1)^n}{(\pi n)^2}\right), \quad n \geqslant 1. \end{aligned} \tag{45}$$

The solution for $\mathcal{H}(\zeta)$ now follows from (33) with coefficients given by (45):

$$\mathcal{H}(\zeta) = \frac{1}{2} + \sum_{n\geqslant 1}^{\infty} \frac{2}{1+\rho^n}\left(\frac{1-(-1)^n}{(\pi n)^2}\right)\left(\zeta^n + \frac{\rho^n}{\zeta^n}\right) + \mathrm{i}c, \quad c \in \mathbb{R}. \tag{46}$$

The imaginary part of $\mathcal{H}(\zeta)$ is not fixed by the modified Schwarz problem. But, from (28), the required Goursat function determining the flow is

$$f(z) = \frac{\mathrm{i}}{4}h(z) = \frac{\mathrm{i}}{4}\left[\frac{1}{2} + \sum_{n\geqslant 1}^{\infty} \frac{2}{1+\rho^n}\left(\frac{1-(-1)^n}{(\pi n)^2}\right)\left(\zeta^n + \frac{\rho^n}{\zeta^n}\right)\right], \tag{47}$$

where the no-slip condition when ζ is on the real axis necessitates the choice $c = 0$. On substitution of the solution (47) for $f(z)$ into (21) with the choice (23) the stream function reported in (71) follows after multiplication by $\beta^\star \Delta T^\star/\mu^\star$.

VII. PUMPING SPEED

Having solved for the flow field, the nondimensional pumping speed, denoted by U_∞, follows by examining its far-field form, i.e., $u - \mathrm{i}v \to U_\infty$ as $y \to \infty$. It follows from (11) that

$$\begin{aligned} u - \mathrm{i}v &= -\overline{f(z)} + \bar{z}f'(z) + g'(z) = -\overline{f(z)} + \bar{z}f'(z) - zf'(z) - f(z) \\ &= -\overline{f(z)} - 2\mathrm{i}yf'(z) - f(z). \end{aligned} \tag{48}$$

Since

$$f(z) \to f_\infty + \mathcal{O}(1/z), \quad \text{as } z \to \infty \tag{49}$$

then $f'(z) \to \mathcal{O}(1/z^2)$ and

$$u - \mathrm{i}v \to -2\mathrm{Re}[f_\infty] \equiv U_\infty, \quad \text{as } y \to \infty. \tag{50}$$

But $\zeta = \alpha$ is the preimage of the point at infinity $y \to \infty$ in the principal period window, so

$$f_\infty = \frac{\mathrm{i}}{4}\left[\frac{1}{2} + \sum_{n\geqslant 1}^{\infty} \frac{2}{1+\rho^n}\left(\frac{1-(-1)^n}{(\pi n)^2}\right)\left(\alpha^n + \frac{\rho^n}{\alpha^n}\right)\right], \tag{51}$$

therefore,

$$U_\infty = -2\mathrm{Re}[f_\infty] = \mathrm{Im}\left[\sum_{n\geqslant 1}^{\infty} \frac{1}{1+\rho^n}\left(\frac{1-(-1)^n}{(\pi n)^2}\right)\left(\alpha^n + \frac{\rho^n}{\alpha^n}\right)\right]. \tag{52}$$

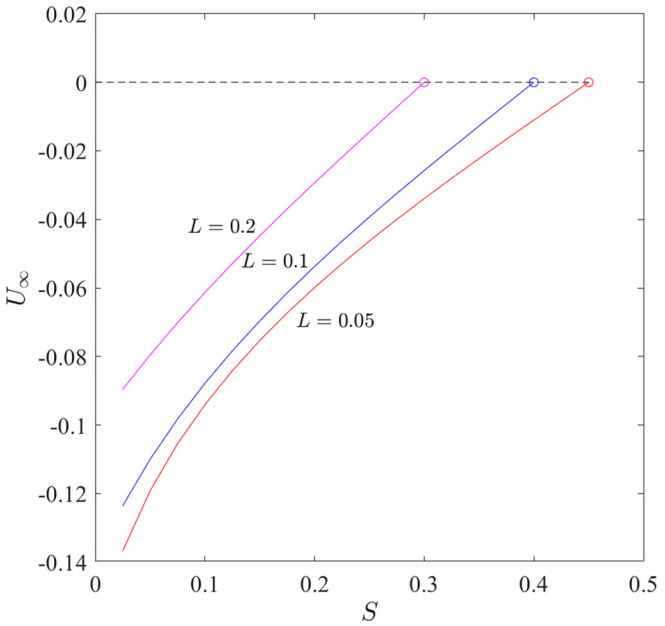

FIG. 4. Dimensionless pumping speeds for plates of equal length $L = 0.05, 0.1$, and 0.2 for different values of the separation parameter S. When $S = (1 - 2L)/2$ the menisci have the same length and there is no pumping ($U_\infty = 0$).

The terms corresponding to even n vanish and we can write $n = 2m - 1$ for $m \geqslant 1$ giving

$$U_\infty = \frac{2}{\pi^2}\mathrm{Im}\left[\sum_{m\geqslant 1}^{\infty}\frac{1}{(2m-1)^2(1+\rho^{2m-1})}\left(\alpha^{2m-1} + \frac{\rho^n}{\alpha^{2m-1}}\right)\right]. \tag{53}$$

But $\alpha = \mathrm{i}r$ so that, for $n = 2m - 1$,

$$\alpha^n = \mathrm{i}(-1)^{m+1}r^{2m-1}, \qquad \frac{\rho^n}{\alpha^n} = \mp\mathrm{i}(-1)^{m+1}\left(\frac{\rho}{r}\right)^{2m-1}. \tag{54}$$

This means

$$U_\infty = \frac{2}{\pi^2}\sum_{m\geqslant 1}^{\infty}\frac{(-1)^{m+1}}{(2m-1)^2(1+\rho^{2m-1})}\left(r^{2m-1} - \left(\frac{\rho}{r}\right)^{2m-1}\right), \tag{55}$$

which is an explicit formula for the nondimensional pumping speed as a function of r and ρ. If $r = \sqrt{\rho}$ inspection of the formula reveals that $U_\infty = 0$ since then all the terms in the sum vanish. This corresponds to the case where the menisci have equal length and there is no pumping, only recirculatory mixing, in the liquid generated by the thermocapillary stress.

Figure 4 shows a graph of U_∞ as a function of the separation parameter S for three different choices of the plate length $L = 0.05, 0.1$, and 0.2. When $S = (1 - 2L)/2$ the menisci have the same length and there is no pumping, as expected. However, as S decreases from this value the liquid is pumped to the left with increasing speed as S decreases. The loss of symmetry between the two menisci is responsible for this net pumping effect. Interestingly, the flow direction is selected by the longer meniscus.

Figure 5, which shows typical streamlines for $L = 0.2$ and for different values of the separation parameter S, illustrates how a pure mixing flow when $S = (1 - 2L)/2 = 0.3$ develops a net pumping component as S gradually decreases from this value.

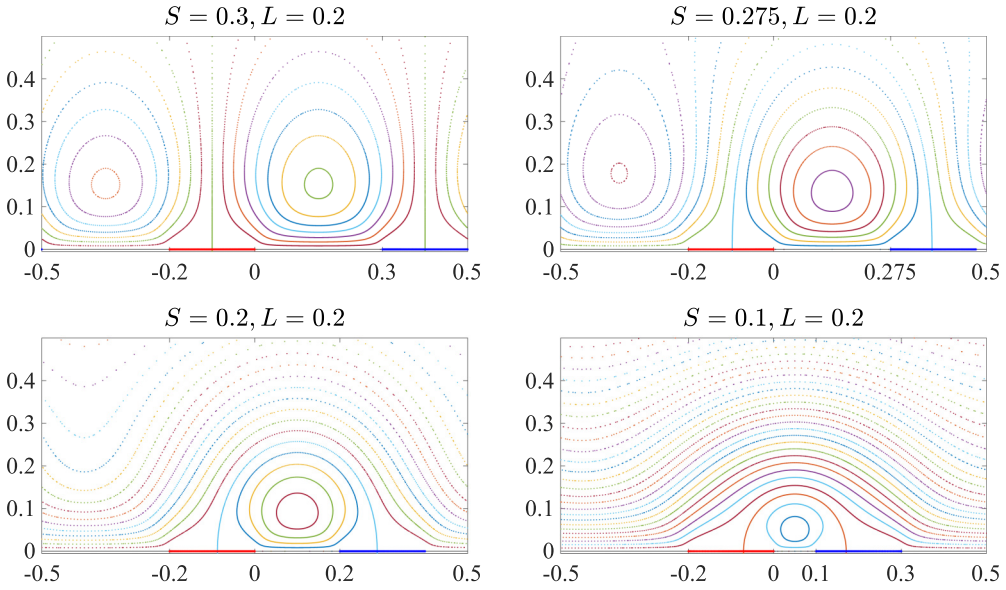

FIG. 5. Streamline distributions showing how a purely recirculating mixing flow develops a net pumping component as the plate separation parameter S decreases from the value $(1 - 2L)/2$ causing the two meniscus portions in each period window to have different lengths. Here $L = 0.2$ so that when $S = 0.3$ the configuration is left-right symmetric and there is thermocapillary-induced mixing but no pumping.

VIII. RECIPROCAL THEOREM

It turns out that another explicit formula for the net pumping speed can be found that is distinct from, but produces the same results as, the formula (55) already found. This formula emerges from the reciprocal theorem for Stokes flow combined with use of previously derived exact solutions for longitudinal flow over a superhydrophobic surface with two no-shear menisci per period [27]. Interestingly, this second formula for the pumping speed can be derived without any need to solve for the flow field. This alternative determination of the pumping speed only requires knowledge of the Marangoni stress on the menisci which might feasibly be caused by many other physical mechanisms besides that due to thermocapillarity as envisaged here. Consequently, the analysis to follow may well be useful in determining the pumping speed for many other problems in the same domain architecture.

The reciprocal theorem for Stokes flow [32] is an integral relation between two solutions of the Stokes equations, $\{u_i, \sigma_{ij}\}$ and $\{\hat{u}_i, \hat{\sigma}_{ij}\}$ say, taking place in the same domain D having boundary ∂D. Specifically,

$$\oint_{\partial D} u_i \hat{\sigma}_{ij} n_j ds = \oint_{\partial D} \hat{u}_i \sigma_{ij} n_j ds, \tag{56}$$

where ds is the arclength element around the boundary and n_i denotes the components of the outward unit normal vector. Suppose now that ∂D is the boundary of a period window for the interdigitated thermocapillary pump. Suppose also that $\{\hat{u}_i, \hat{\sigma}_{ij}\}$ is the solution to a problem akin to the thermocapillary pump problem where $M^{(k)}(x)$ denotes the Marangoni stress on the kth meniscus and suppose that $\{u_i, \sigma_{ij}\}$ is the "comparison solution" associated with simple transverse shear flow, with unit shear rate, over a periodic superhydrophobic surface with the same geometry and with two shear-free menisci per period. On use of the periodicity of both solutions, which means that all contributions to both integrals from the sides of the period window cancel out, the only contribution to the integral on the right-hand side arises from $y \to \infty$ and equals $-U_\infty$. Similarly, the only

nonzero contributions to the left-hand-side integral are

$$\int_{\text{meniscus 1}} U_1(x)M^{(1)}(x)dx + \int_{\text{meniscus 2}} U_2(x)M^{(2)}(x)dx, \tag{57}$$

where $U_i(x)$ for $i = 1, 2$ are the tangential slip velocities on the two shear-free menisci in the comparison solution. This results in the equation

$$U_\infty = -\int_{\text{meniscus 1}} U_1(x)M^{(1)}(x)dx - \int_{\text{meniscus 2}} U_2(x)M^{(2)}(x)dx, \tag{58}$$

which is a formula for the pumping speed U_∞ for *any* given interfacial Marangoni stresses (not just those relevant to the thermocapillary pump of interest here) provided $U_i(x)$ for $i = 1, 2$ are known. But a solution to the comparison problem has been found, in analytical form, by Crowdy [27] in a study of superhydrophobic surfaces having more than one shear-free meniscus per period. Formula (58), in combination with the exact solution of Crowdy [27], therefore provides a valuable formula for the pump speed due to *any* form of imposed Marangoni stress.

Since this paper has adopted a complex variable formulation, all that remains is to rephrase formula (56) in the same language. Since, in complex variable notation,

$$u_i\sigma_{ij}n_j \mapsto \text{Re}\left[(u - \text{i}v)\left(-2\text{i}\frac{dH}{ds}\right)\right], \tag{59}$$

where $H(z, \bar{z}) = f(z) + z\overline{f'(z)} + \overline{g'(z)}$ [27,29], then the reciprocal theorem (56) can also be stated as

$$\int_{\partial D} \text{Re}[(u - \text{i}v)(-2\text{i}d\hat{H})] = \int_{\partial D} \text{Re}[(\hat{u} - \text{i}\hat{v})(-2\text{i}dH)]. \tag{60}$$

On $y = 0$,

$$u - \text{i}v = -2\text{Re}[f(z)], \quad \hat{u} - \text{i}\hat{v} = -2\text{Re}[\hat{f}(z)], \tag{61}$$

and

$$H = 2\text{iIm}[f(z)], \quad \hat{H} = 2\text{iIm}[\hat{f}(z)]. \tag{62}$$

The form of $f(z)$ relevant to the problem of transverse flow, with unit shear rate, over a superhydrophobic surface comprising two shear-free menisci in each period window occupying the same intervals as the menisci in the thermocapillary pump was determined in [27] to be

$$f(z) = -\frac{1}{8\pi}\log\left(\frac{P(\zeta/\alpha, \rho)P(\zeta\overline{\alpha}, \rho)}{P(\zeta/\overline{\alpha}, \rho)P(\zeta\alpha, \rho)}\right). \tag{63}$$

Interestingly, the same function $P(\zeta, \rho)$, defined in (9) and appearing in the conformal mapping function, also appears in formula (63) for $f(z)$. Note that, as required by the superhydrophobic surface problem,

$$f(z) \to \frac{\text{i}z}{4}, \quad \text{as } y \to \infty. \tag{64}$$

Consequently, the statement (60) of the reciprocal theorem becomes

$$\int_{-1/2}^{1/2} \text{Re}[f(z)]\text{Im}[d\hat{f}(z)] = \int_{-1/2}^{1/2} \text{Re}[\hat{f}(z)]\text{Im}[df(z)] - \left(\frac{U_\infty}{2} \times \frac{1}{4}\right), \tag{65}$$

where the facts that, as $y \to \infty$, $\text{Im}[df(z)] = dx/4$ and $-2\text{Re}[f(z)] \to U_\infty$ have been used. But this simplifies to

$$\int_{-1/2}^{1/2} \text{Re}[f(z)]\text{Im}[d\hat{f}(z)] = -\frac{U_\infty}{8} \tag{66}$$

because $\mathrm{Re}[\hat{f}(z)] = 0$ on the no-slip walls and $\mathrm{Im}[df(z)] = 0$ on the menisci: recall that, in the superhydrophobic surface problem considered in [27] the menisci are free of shear, and it is this feature that makes it the ideal choice of comparison problem here. The Marangoni condition (25) for the thermocapillary pump problem is

$$-2\mathrm{i}\frac{d\hat{H}}{dx} = -\frac{\partial\sigma}{\partial x} = \frac{\partial T}{\partial x}, \quad \text{or} \quad -2\mathrm{i}d\hat{H} = dT \tag{67}$$

and $\hat{H} = 2\mathrm{i}\mathrm{Im}[\hat{f}(z)]$, hence

$$4\mathrm{Im}[d\hat{f}(z)] = dT. \tag{68}$$

But from the complex potential (71) for the temperature field, and since χ is constant on the menisci,

$$\mathrm{i}dT = -\frac{d\zeta}{\pi\zeta}, \quad \text{or} \quad dT = -\frac{d\zeta}{\mathrm{i}\pi\zeta}. \tag{69}$$

Hence

$$4\mathrm{Im}[d\hat{f}(z)] = -\frac{d\zeta}{\mathrm{i}\pi\zeta}. \tag{70}$$

Finally, on use of (63) and (70) in (66), and on writing the integral over C_0^+ and C_1^+ (traversed anticlockwise) and multiplying by $\beta^\star\Delta T^\star/\mu^\star$, the formula (73) reported in the next section emerges.

IX. SUMMARY OF THEORETICAL RESULTS

It is useful to summarize the main theoretical results in dimensional form. It has been shown here that the stream function $\psi^\star$ associated with a model of the Marangoni-induced flow of a viscosity-$\mu^\star$ liquid and the associated temperature field $T^\star$ causing the thermocapillary stress are given parametrically, in terms of a parametric complex variable ζ sitting in an upper-half annulus $\rho < |\zeta| < 1$, $\mathrm{Im}[\zeta] > 0$, by the explicit formulas

$$\begin{aligned}
\psi^\star &= \mathrm{Im}\left[(\overline{Z^\star(\zeta)} - Z^\star(\zeta))\frac{\mathrm{i}\beta^\star\Delta T^\star}{4\mu^\star}\left[\frac{1}{2} + \sum_{n\geqslant 1}^{\infty}\frac{2}{1+\rho^n}\left(\frac{1-(-1)^n}{(\pi n)^2}\right)\left(\zeta^n + \frac{\rho^n}{\zeta^n}\right)\right]\right],\\
T^\star &= \mathrm{Im}\left[\Delta T^\star\left(\mathrm{i} - \frac{1}{\pi}\log\zeta\right)\right],\\
z^\star &= x^\star + \mathrm{i}y^\star = Z^\star(\zeta) = -\frac{\mathrm{i}D^\star}{2\pi}\log\left[R\,\frac{P(\zeta/\alpha,\rho)P(\zeta\alpha,\rho)}{P(\zeta/\overline{\alpha},\rho)P(\zeta\overline{\alpha},\rho)}\right], \quad \alpha = \mathrm{i}r,
\end{aligned} \tag{71}$$

where $\Delta T^\star$ is the temperature difference between the hot and cold combs, $\beta^\star$ captures the effect of temperature change on surface tension, $D^\star$ is the period length, and $P(\zeta,\rho)$ is a special function associated with the annulus and defined in (9). The $\star$ superscripts signify dimensional parameters. The two nondimensional mathematical parameters ρ and r are determined from the geometry of the device architecture by solving (11).

A formula (55) for the pumping speed $U_\infty^\star$ follows directly from the full solution (71) and in dimensional form is

$$U_\infty^\star = \frac{\beta^\star\Delta T^\star}{\mu^\star} \times \frac{2}{\pi^2}\sum_{m\geqslant 1}^{\infty}\frac{(-1)^{m+1}}{(2m-1)^2(1+\rho^{2m-1})}\left(r^{2m-1} - \left(\frac{\rho}{r}\right)^{2m-1}\right). \tag{72}$$

An equivalent alternative formula, derived from the reciprocal theorem in Sec. VIII, is

$$U_\infty^\star = \frac{\beta^\star\Delta T^\star}{\mu^\star} \times \left(-\frac{1}{4\pi^2}\right) \times \left(\int_{C_0^+} - \int_{C_1^+}\right)\log\left|\frac{P(\zeta/\alpha,\rho)P(\zeta\overline{\alpha},\rho)}{P(\zeta/\alpha,\rho)P(\zeta\overline{\alpha},\rho)}\right|\frac{d\zeta}{\mathrm{i}\zeta}. \tag{73}$$

It can be checked numerically that the integral expression (73) gives the same result as expression (72). This provides reassuring corroborating checks on both analytical approaches.

Numerical corroboration

As a check on the derived analytical solutions, the model problem was additionally solved numerically. A two-dimensional Chebyshev pseudospectral method was used. The periodic domain was split into four (or five) subdomains, one over each meniscus, one above the hot plate and another above the cold plate (two if the cold plate was split by the period line). Each subdomain was then discretized into an $N \times M$ collocation grid with Gauss-Lobatto spacing in both directions. Since the temperature field is independent of the velocity field in the zero Péclet number limit, it was found first. A $5MN \times 5MN$ matrix, denoted by A, was constructed by satisfying Laplace's equation on the interior points and the relevant boundary conditions at boundary points. Solving for the temperature then reduces to solving the matrix system

$$A\vec{T}_{\text{num}} = \vec{F}_{\text{num}}, \tag{74}$$

where $\vec{T}_{\text{num}}$ is a vector containing the unknown temperatures at the collocation points and F_{num} is a forcing vector and nonzero only at points corresponding to the hot plate. The linear system is readily solved using standard methods.

After determining $\vec{T}_{\text{num}}$, the thermocapillary stress can be extracted and fed into a steady-state solver for the hydrodynamic problem. A vorticity-stream-function formulation is used to avoid solving the fourth-order Stokes equations. Since this requires finding two unknowns, ψ_{num} and ω_{num}, the numerical stream function and vorticity, respectively, the resulting matrix system has size $10MN \times 10MN$ but it is similarly solvable using standard methods.

To compare the numerical solution with its analytical counterpart, the average velocity of the numerical solution was calculated far from the composite interface. This gives a numerical estimate of U_∞. Agreement with the analytical solution is excellent, but to achieve good accuracy the truncation choices $N = 21$ and $M = 31$ are necessary, resulting in the need to invert large matrices. This underscores the value in having available an analytical solution (72), especially for purposes of device optimization involving extensive calculations over design parameter sweeps.

Finally, to assess the domain of validity of our model, the numerical code described above was adapted to allow for solutions at arbitrary Pe. This was done by adding a pseudotime to the temperature problem and running the modified code until a steady state was reached.

X. DEVICE METRICS

There are two parameters of chief importance in quantifying the engineering viability of the thermocapillary pump: the pumping speed, $U_\infty^\star$, and the heat load per unit depth required along the hot ridge, which we call $q_{\text{c}}^{\star\prime}$. The heat load is obtaining by integrating the normal derivative of the temperature field over the hot ridge and multiplying by the thermal conductivity of the liquid $k_{\text{l}}^\star$, according to Fourier's law:

$$q_{\text{c}}^{\star\prime} = -\int_{-L^\star}^{0} k_{\text{l}}^\star \frac{\partial T^\star}{\partial y^\star} \mathrm{d}x^\star. \tag{75}$$

Only the heat load associated with the hot ridge is relevant since this is the only actively heated element (see Fig. 2). This merits introduction of a dimensionless heat load $q_{\text{c}}' = q_{\text{c}}^{\star\prime}/(k_{\text{l}}^\star \Delta T^\star)$, which is independent of the period length $D^\star$ due to the integration along the ridge. On plugging the dimensionless parameters into (75), and using one of the Cauchy-Riemann equations, it follows that

$$q_{\text{c}}' = -\frac{1}{\pi} \log \rho. \tag{76}$$

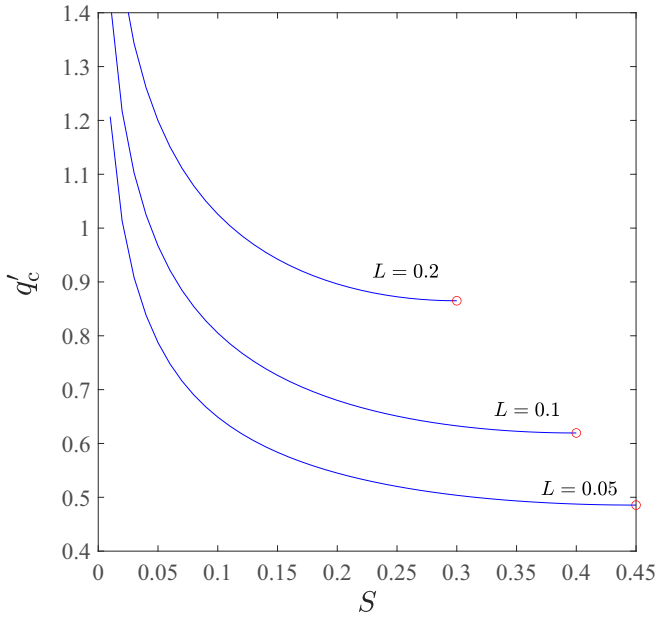

FIG. 6. Nondimensionalized heat load for plates of equal length $L = 0.05$, 0.1, and 0.2 for different values of the separation parameter S.

Of interest is the relationship between the geometric parameters S and L and the two parameters U_∞ and q'_c. Figure 4, already discussed in Sec. VII, shows that $|U_\infty|$ increases monotonically as both $S \to 0$ and $L \to 0$. This implies that pumping speed will be maximized when both S and L are small. To prompt a similar qualitative analysis for the heat load, Fig. 6 depicts the effect of S and L on q'_c. It shows that $|q'_c|$ increases monotonically as $S \to 0$, but decreases as $L \to 0$. These observations are both unsurprising. First, if L is held constant as $S \to 0$, the two isothermal ridges approach each other and the temperature field becomes more singular, increasing the heat load. Conversely, if S is held constant and $L \to 0$, the total available area of heat transfer vanishes, reducing the heat load.

To summarize the relationships, $|U_\infty|$ increases and $|q_c|$ decreases as $L \to 0$, implying that smaller L are always preferable. Conversely, both increase as $S \to 0$, which suggests a competition between pumping power and heat load. To examine this competition we define an efficiency parameter, $E = U_\infty/q'_c$, which is the dimensionless ratio of pumping speed to pumping power. Figure 7 shows E for different values of L and S.

Notably, there is a value of S, designated by S_{opt}, that yields a maximum efficiency for each choice of L. This happens because although $|U_\infty|$ increases as $S \to 0$, the heat load required increases much faster, reducing efficiency. A root finder was used to calculate S_{opt} for a chosen L. The results are plotted in the inset of Fig. 7. Interestingly, S_{opt} itself has a maximum at $L \approx 0.0875$. This shows there is a maximum spacing length for all L above which E is always nonoptimal.

Illustrative calculations

This section documents some example calculations and tests some of the limits of our assumptions. In view of the previous section, the values of the geometric parameters corresponding to the maximum value of S_{opt} are chosen, that is, $L = 0.0875$ and $S = 0.058$. With this S and L, and solving (72), it is found that the dimensionless pumping speed is $|U_\infty| = 0.109$. Solving (76) gives the dimensionless heat load as $|q'_c| = 0.893$. We can then turn to the dimensional values of the parameters. To obtain $U^\star_\infty$ and $q^{\star\prime}_c$ their dimensionless forms must be multiplied by $\beta^\star \Delta T^\star/\mu^\star$ and $k^\star_l \Delta T^\star$, respectively. If the liquid is taken to be water then $\mu^\star = 10^{-3}$ kg m/s, $k^\star_l = 0.598$

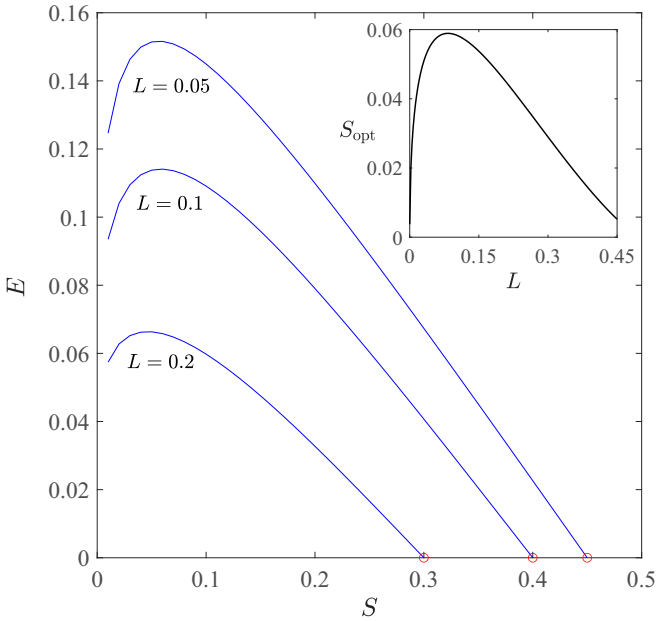

FIG. 7. Efficiency parameter for equal plates of length $L = 0.05$, 0.1, and 0.2 for different values of the separation parameter S. Inset: S_{opt} for different values of the ridge length parameter L.

W m^{-1} K^{-1}, and $\beta^\star = 1.65\times10^{-4}$ N m^{-1} K^{-1} [33]. With $\Delta T^\star = 1\,^\circ$C, the result is $|U_\infty^\star| = 0.018$ m s^{-1} and $|q_c^\star| = 0.534$ W m^{-1}. These dimensional values are both independent of $D^\star$: the role of $D^\star$ is simply to inform how many periods there are, which plays a role in the total amount of power required for the pump. For example, if the microchannel is assumed to be 2 cm long and 1 cm wide, then with $D^\star = 200$ μm there are a total of 100 ridges to heat. The total heat load is then 0.534 W. Dividing by the area of the microchannel, this gives a heat flux of 26.8 W m^{-2}. If, however, the period length is 2 mm there are only 10 hot ridges per channel and the heat load required is reduced to 0.0534 W and the heat flux to 2.68 W m^{-2}. These heat fluxes are far below the onset of boiling.

By way of comparison, returning to the numerical portion of the Baier *et al.* [15] study, further described in [34], recall that a linear drop in temperature between neighboring ridges yields a thermocapillary stress that pumps the flow. This full problem was solved by those authors in COMSOL capturing both inertial and advective effects, which the model here has ignored. When the free surface fraction, defined as meniscus length divided by period length, is 0.8, Baier *et al.* [15] found temperature gradients of 600 °C m^{-1} and 1900 °C m^{-1} generated far-field flow rates of water of 1.7 and 3.2 mm/s, respectively. For our geometry, an analog to this temperature gradient parameter is $\Delta T^\star/D^\star$. Assuming $D^\star = 50$ μm, the $\Delta T^\star$ corresponding to the two temperature gradients is $\Delta T^\star = 0.03\,^\circ$C and $\Delta T^\star = 0.095\,^\circ$C. Since a free surface fraction of 0.8 corresponds to when $L = 0.1$ we can solve for $U_\infty^\star$ to compare. The value $S = 0.0584$ is chosen to maximize the efficiency. If the liquid is taken to be water the values $U_\infty^\star = 0.524$ mm/s and $U_\infty^\star = 1.66$ mm/s are found for the two different temperatures. This indicates that the asymmetric pump proposed here can achieve at least the same order of magnitude of flow rate as the alternative pump suggested by Baier *et al.* [34]. Moreover, the asymmetric pump has the advantage that the average liquid temperature does not change as the flow travels downstream. This means there is no limitation on the channel length (due to freezing) and that, in practice, $\Delta T^\star/D^\star$ can be set to significantly higher values than the temperature gradient in [34], resulting in higher velocities. For example, setting $\Delta T^\star = 0.3\,^\circ$C means $U_\infty^\star = 5.24$ mm/s. However, this corresponds to a temperature gradient of 6000 °C m^{-1} in the pump proposed in [34] where the temperature of a 2-cm channel would decrease from 100 °C

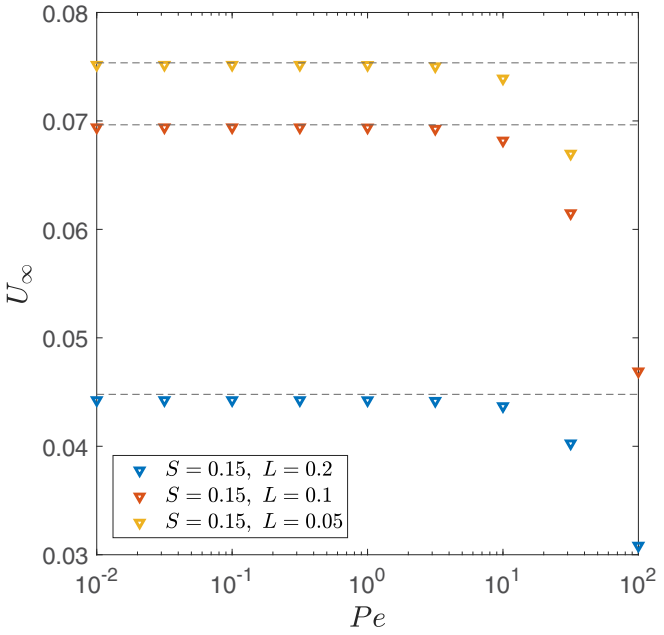

FIG. 8. Dimensionless pumping speeds for plates of equal length with $L = 0.05$, 0.1, and 0.2 and $S = 0.15$ for different values of Pe. The dashed lines show results from the analytical solutions given by (72).

at the inlet to a physically unrealistic $-20\,^\circ$C. One area of concern with the analytical model are the assumptions of zero Pe and Re as U_∞ gets larger. Using the definitions of Re and Pe from the problem statement (with $U^\star = \beta^* \Delta T^* / \mu^*$) and taking $\rho^\star = 997\ \mathrm{kg/m^3}$ and $\alpha^\star = 0.14 \times 10^{-6}\ \mathrm{m^2/s}$ then the values of these parameters for the two cases discussed in [26] are $\mathrm{Re} = 0.25$ and $\mathrm{Pe} = 1.77$ when $\Delta T^* = 0.03\,^\circ$C and $\mathrm{Re} = 0.78$ and $\mathrm{Pe} = 5.60$ when $\Delta T^* = 0.095\,^\circ$C. These last values, particularly the nearly $O(10)$ value of Pe, call into question the assumptions in our analytical model. Figure 8 shows the results of numerical simulations aimed at testing the small-Pe assumption; it shows that the analytical model is a good estimate of Pe of up to about 10. This has two implications on the results discussed in this section. The first is that the estimates of $U_\infty^\star$ when $\Delta T^* = 0.03\,^\circ$C and $\Delta T^* = 0.095\,^\circ$C should be fairly accurate as they both have $\mathrm{Pe} < 10$. The second is that the $U_\infty^\star = 5.24$ mm/s case calculated when $\Delta T^\star = 0.3\,^\circ$C is probably an idealized upper bound since in this case $\mathrm{Pe} = 17.7$.

Interestingly, Fig. 8 shows that the pumping speed decreases as the Pe number increases. This happens because the increased advection moves thermal energy from the hot plate towards the cold plate which, although the average temperature gradient across each meniscus remains constant, reduces the temperature gradient in the center of the menisci when compared to the zero-Pe case. Consequently, the portion of the meniscus that causes substantial shear stresses is decreased and the Marangoni stress becomes contained in small areas close to the edges of the meniscus. A shear stress acting on a small area will generate smaller far-field flow rates than a stress acting on a larger area if the average shear stress of the two cases is identical. Therefore, the increased containment of the temperature gradients as Pe increases manifests itself as a smaller pumping speed.

Other liquids may be considered as well. For example, Galinstan, a nontoxic replacement for mercury under consideration for the thermal management of electronics [35,36], or mercury itself, may be pumped. Notably, the surface tension of mercury is a stronger function of temperature than that of water; e.g., it drops 40% more between 15 °C and 50 °C [37]. And the use of liquid metals has other implications. First, they are nonvolatile; consequently, phase change (evaporation and condensation) along menisci, especially near triple-contact lines, will negligibly change the

temperature and velocity profiles (compared with water, where it produces a substantial effect for sufficiently large $\Delta T^\star$; see [38]). Second, for degassed systems, the absence of a subphase (e.g., water vapor in the case of water substantially above room temperature) implies no adverse shear stresses are exerted by it along menisci. Furthermore, liquid metals may be heated to much higher temperatures before transitioning to pure vapor (e.g., the saturation temperature of Galinstan at ambient pressure is above 1300 °C according to a tabulation of its properties in [35]); consequently, much stronger thermocapillary stresses may be imposed. One drawback of Galinstan is that, due to its higher thermal conductivity, more power is required to obtain the same temperature difference along a meniscus. Finally, menisci in liquid metals may be less susceptible to immobilization via the presence of surfactants as may occur with water, especially if they are short [39].

XI. CONCLUSION

The theoretical thermocapillary pump put forward here has all the same advantages of the electro-osmotic pump proposed by Adjari [3]. It has no moving parts and the asymmetry responsible for pumping is built into the fixed device architecture and does not rely, for example, on the continuous production of discrete droplets as required in many devices that leverage electrowetting effects. Moreover, it does not require the imposition of an external pressure gradient, or any other external electric field or thermal gradient; indeed the device is thermally adiabatic with no net heat generated in any period window. As a consequence, there is no physical limitation on the length of this pump beyond total energy consumed, making it attractive for applications where large pumping distances are required.

Finally, a conceptual design of the pump has been outlined in order to guide a future experimental study. The present paper has demonstrated its theoretical viability. Work is in progress to build such a pump with Fig. 2 illustrating one of many design ideas for its practical realization.

ACKNOWLEDGMENTS

This work was partly supported by the Engineering and Physical Sciences Research Council (EP/V062298/1) as well as the National Science Foundation through the Division of Chemical, Bioengineering, Environmental, and Transport Systems under Grant No. 2140033. Dr. Hy Dinh produced Fig. 2. The authors thank Prof. Vaibhav Bahadur for bringing their attention to Ref. [3].

[1] T. M. Squires and S. R. Quake, Microfluidics: Fluid physics at the nanoliter scale, Rev. Mod. Phys. **77**, 977 (2005).

[2] H. A. Stone, A. D. Stroock, and A. Ajdari, Engineering flows in small devices: Microfluidics toward a lab-on-a-chip, Annu. Rev. Fluid Mech. **36**, 381 (2004).

[3] A. Ajdari, Pumping liquids using asymmetric electrode arrays, Phys. Rev. E **61**, R45(R) (2000).

[4] A. B. D. Brown, C. G. Smith, and A. R. Rennie, Pumping of water with ac electric fields applied to asymmetric pairs of microelectrodes, Phys. Rev. E **63**, 016305 (2000).

[5] V. Studer, A. Pépin, Y. Chen, and A. Ajdari, Fabrication of microfluidic devices for AC electrokinetic fluid pumping, Microelectron. Eng. **61–62**, 915 (2002).

[6] M. Mpholo, C. G. Smith, and A. B. D. Brown, Low voltage plug flow pumping using anisotropic electrode arrays, Sens. Actuators B: Chem. **92**, 262 (2003).

[7] A. Ramos, A. González, A. Castellanos, N. G. Green, and H. Morgan, Pumping of liquids with ac voltages applied to asymmetric pairs of microelectrodes, Phys. Rev. E **67**, 056302 (2003).

[8] T. M. Squires and M. Z. Bazant, Breaking symmetries in induced charge electroosmosis and electrophoresis, J. Fluid Mech. **560**, 65 (2006).

[9] T. S. Sammarco and M. A. Burns, Thermocapillary pumping of discrete drops in microfabricated analysis devices, AIChE J. **45**, 350 (1999).

[10] D. E. Kataoka and S. M. Troian, Patterning liquid flow on the microscopic scale, Nature (London) **402**, 794 (1999).
[11] A. Würger, Thermally driven Marangoni surfers, J. Fluid Mech. **752**, 589 (2014).
[12] A. Karbalaei, K. Ranganathan, and J. Cho, Thermocapillarity in microfluidics—A review, Micromachines **7**, 13 (2016).
[13] V. Frumkin, K. Gommed, and M. Bercovici, Dipolar thermocapillary motor and swimmer, Phys. Rev. Fluids **4**, 074002 (2019).
[14] A. Strook, R. Ismagilov, H. Stone, and G. Whitesides, Fluidic ratchet based on Marangoni-Bénard convection, Langmuir **19**, 4358 (2003).
[15] T. Baier, C. Steffes, and S. Hardt, Thermocapillary flow on superhydrophobic surfaces, Phys. Rev. E **82**, 037301 (2010).
[16] G. Amador, Z. Ren, A. Tabak, Y. Alapan, O. Yasa, and M. Sitti, Temperature gradients drive bulk flow within microchannel lined by fluid-fluid interfaces, Small **15**, 1900472 (2015).
[17] A. Gao, H. J. Butt, W. Steffen, and C. Schönecker, Optical manipulation of liquids by thermal Marangoni flow along the air-water interfaces of a superhydrophobic surface, Langmuir **37**, 8677 (2021).
[18] M. Hodes, T. Kirk, G. Karamanis, and S. MacLachlan, Effect of thermocapillary stress on slip length for a channel textured with parallel ridges, J. Fluid Mech. **814**, 301 (2017).
[19] T. Kirk, G. Karamanis, D. Crowdy, and M. Hodes, Thermocapillary stress and meniscus curvature effects on slip lengths in ridged microchannels, J. Fluid Mech. **894**, A15 (2020).
[20] E. Yariv, Thermocapillary flow between longitudinally grooved superhydrophobic surfaces, J. Fluid Mech. **855**, 574 (2018).
[21] E. Yariv and D. G. Crowdy, Thermocapillary flow between grooved superhydrophobic surfaces: Transverse temperature gradients, J. Fluid Mech. **871**, 775 (2019).
[22] E. Yariv and D. G. Crowdy, Longitudinal thermocapillary flow over a dense bubble mattress, SIAM J. Appl. Math. **80**, 1 (2020).
[23] E. Yariv and T. Kirk, Longitudinal thermocapillary slip about a dilute periodic mattress of protruding bubbles, IMA J. Appl. Math. **86**, 490 (2021).
[24] S. Tomlinson, M. Mayer, T. Kirk, M. Hodes, and D. Papageorgiou, Thermal resistance of heated superhydrophobic channels with streamwise thermocapillary stress, ASME J. Heat Mass Transfer. (to be published).
[25] R. S. Hale and V. Bahadur, Electrowetting heat pipes for heat transport over extended distances, IEEE Trans. Compon. Packaging Manuf. Technol. **5**, 1441 (2015).
[26] R. S. Hale and V. Bahadur, Electrowetting-based microfluidic operations on rapid-manufactured devices for heat pipe applications, J. Micromech. Microeng. **27**, 075004 (2017).
[27] D. G. Crowdy, Frictional slip lengths for unidirectional superhydrophobic grooved surfaces, Phys. Fluids **23**, 072001 (2011).
[28] D. G. Crowdy, Solving problems in multiply connected domains, in *NSF-CBMS Regional Conference Series in Applied Mathematics* (Society for Industrial and Applied Mathematics, Philadelphia, 2020).
[29] D. G. Crowdy, Collective viscous propulsion of a two-dimensional flotilla of Marangoni boats, Phys. Rev. Fluids **5**, 124004 (2020).
[30] D. G. Crowdy, Exact solutions for the formation of stagnant caps of insoluble surfactant on a planar free surface, J. Eng. Math. **131**, 10 (2021).
[31] D. G. Crowdy, The Schwarz problem in multiply connected domains and the Schottky-Klein prime function, Complex Var. Elliptic Equations **53**, 221 (2008).
[32] H. Masoud and H. A. Stone, The reciprocal theorem in fluid dynamics and transport phenomena, J. Fluid Mech. **879**, P1 (2019).
[33] E. W. Lemmon, I. H. Bell, M. L. Huber, and M. O. McLinden, Thermophysical properties of fluid systems, in *NIST Chemistry WebBook, NIST Standard Reference Database Number 69*, edited by P. J. Linstrom and W. G. Mallard (National Institute of Standards and Technology, Gaithersburg MD, 2023).
[34] T. Baier, C. Steffes, and S. Hardt, Numerical modelling of thermocapillary flow on superhydrophobic surface, in *Proceedings of the 14th International Conference on Miniaturized Systems for Chemistry and Life Sciences* (Chemical and Biological Microsystems Society, San Diego, 2010), pp. 1799–1801.

[35] M. Hodes, R. Zhang, L. Lam, R. Wilcoxon, and N. Lower, On the potential of Galinstan-based minichannel and minigap cooling, IEEE Trans. Compon. Packaging Manuf. Technol. **4**, 46 (2014).

[36] R. Zhang, M. Hodes, N. Lower, and R. Wilcoxon, Water-based microchannel and Galinstan-based minichannel cooling beyond $1\,\mathrm{kW/cm^2}$ heat flux, IEEE Trans. Compon. Packaging Manuf. Technol. **5**, 762 (2015).

[37] G. Perry and N. Roberts, Surface tension of mercury between 15 and 50°C by the sessile drop method, J. Chem. Eng. Data **26**, 266 (1981).

[38] M. Hodes, L. Lam, A. Cowley, R. Enright, and S. MacLachlan, Effect of evaporation and condensation at menisci on apparent thermal slip, ASME J. Heat Trans. **137**, 071502 (2015).

[39] F. Peaudecerf, J. Landel, R. Goldstein, and P. Luzzatto-Fegiz, Traces of surfactants can severely limit the drag reduction of superhydrophobic surfaces, Proc. Natl. Acad. Sci. USA **114**, 7254 (2017).